

Geochemistry and petrology of dolerite sills in the Huab River Valley, Damaraland, north-western Namibia

A.R. Duncan, S.R. Newton, C. van den Berg and D.L. Reid

Department of Geochemistry, University of Cape Town, Rondebosch 7700, South Africa

Dolerite sills in the western portion of the Huab River Valley have an outcrop area in excess of 600 km² and individual sills are up to 130 m thick. They intrude both the Damara basement and overlying Karoo Sequence sediments and are frequently transgressive. The sills and associated dykes are separated into four distinct dolerite magma types which are distinguished from each other by different ratios of incompatible element abundances. All the dolerite types are tholeiitic, containing both normative hypersthene and olivine. They are relatively primitive in character with rather high concentrations of Mg, Ni and Cr and low concentrations of incompatible trace elements (e.g. Ba, Zr, and Nb). The Huab sills are compositionally different from the basaltic lavas of the overlying Etendeka Formation and from most of the dolerite types which intrude the lavas. They are closest in composition to the Horingbaai dolerites, a suite of late-stage intrusives into the Etendeka Formation with MORB affinities. The compositional variations within individual sills are consistent with crystal fractionation processes which appear to have operated both by gravitational separation and accumulation of early-formed phenocrysts, and by flow differentiation.

Geological setting

The basement rocks in the western portion of the Huab River valley (west of longitude 14°15' E) are schists of the Pan-African Damara Sequence. The Karoo-age sediments which overlie the basement in this area have been described by Hodgson and Botha (1975) and are now considered to be part of the Dwyka, Prince Albert, Gai-As and Etjo Formations (SACS, 1980). The Etjo Formation is overlain by the volcanic rocks of the Etendeka Formation which in this area consist of Tafel-

berg-type basalts (Erlank *et al.*, 1984) interbedded with two Lower Springbok quartz latite units and capped by the Upper Springbok quartz latite (Milner, 1988). There is limited interbedding of the earliest basalts of the Etendeka Formation with aeolian sandstones of the Etjo Formation.

The occurrence of a major sill in the Huab valley was noted by Hodgson and Botha (1975) and the outcrop area shown in some detail by them as well as on the 1 : 250 000 Cape Cross geological map (Miller, 1988). Botha and Hodgson (1976) suggested that the dolerite in the Huab valley was a single large sill with an outcrop area of at least 400 km² and thickness of up

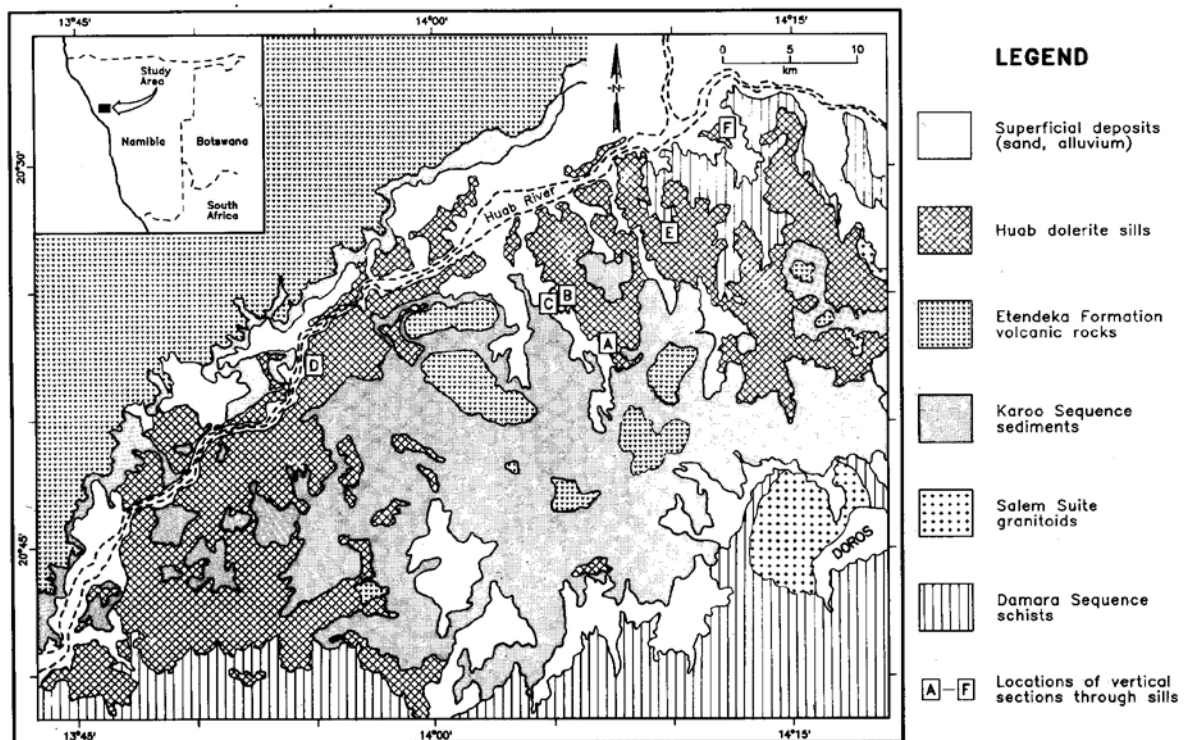


Fig. 1: Simplified geological map of part of the Huab River Valley, Damaraland.

to 100 m. However, the present study has shown that there area number of sills intruded at approximately the same stratigraphic level, rather than a single sill. Their outcrop area is mainly along the Huab River and to its south, the outcrop area to the north of the river being limited in extent. The total outcrop area of the sills as measured from Fig. 1 and from Miller (1988) is approximately 600 km².

The area in which samples were collected for this study is shown in Fig. 1. Within this study area the sills are typically intrusive into Karoo Sequence sediments, normally into the Etjo Formation. In the north-east portion 'of the area a sill is intrusive into the Damara schists. The sills are frequently transgressive and discordant contacts have been observed in many localities. Only one locality has been observed at which a sill intrudes the volcanics of the Etendeka Formation. In this instance the sill intrudes one of the earliest basalt flows which has filled a pre-existing valley in the dune palaeotopography at the top of the Etjo Formation.

Although different dolerite types may be distinguished on the basis of composition, most varieties are essentially identical in hand specimen. This characteristic, combined with transgressive contacts and discontinuous exposure make it difficult to establish how

many discrete sills occur in the study area.

Vertical sections through the sill(s) were sampled at six different localities (shown on Fig. 1), with 5-10 samples taken from each section. The maximum sill thickness in a measured and sampled section was 115 m and at this locality the upper contact of the sill has been removed by erosion. Additional dolerite samples were also collected from dykes and from several small sills within the study area.

Composition and classification

Sixty three dolerite samples from the study area were analysed for major elements and 19 trace elements using X-ray Fluorescence techniques as described by Duncan *et al.*, (1984) and Le Roex (1985).

Examination of the major and trace element data indicates that there are four different compositional groups (Fig. 2). It is important to note that in all cases it is not merely the abundances of elements which are different in different groups but that there are clearly differences in the magnitude of ratios of incompatible element abundances. In this regard it should be noted that in the absence of early-crystallising sulphides in these rocks, Cu behaves as an incompatible element. The different

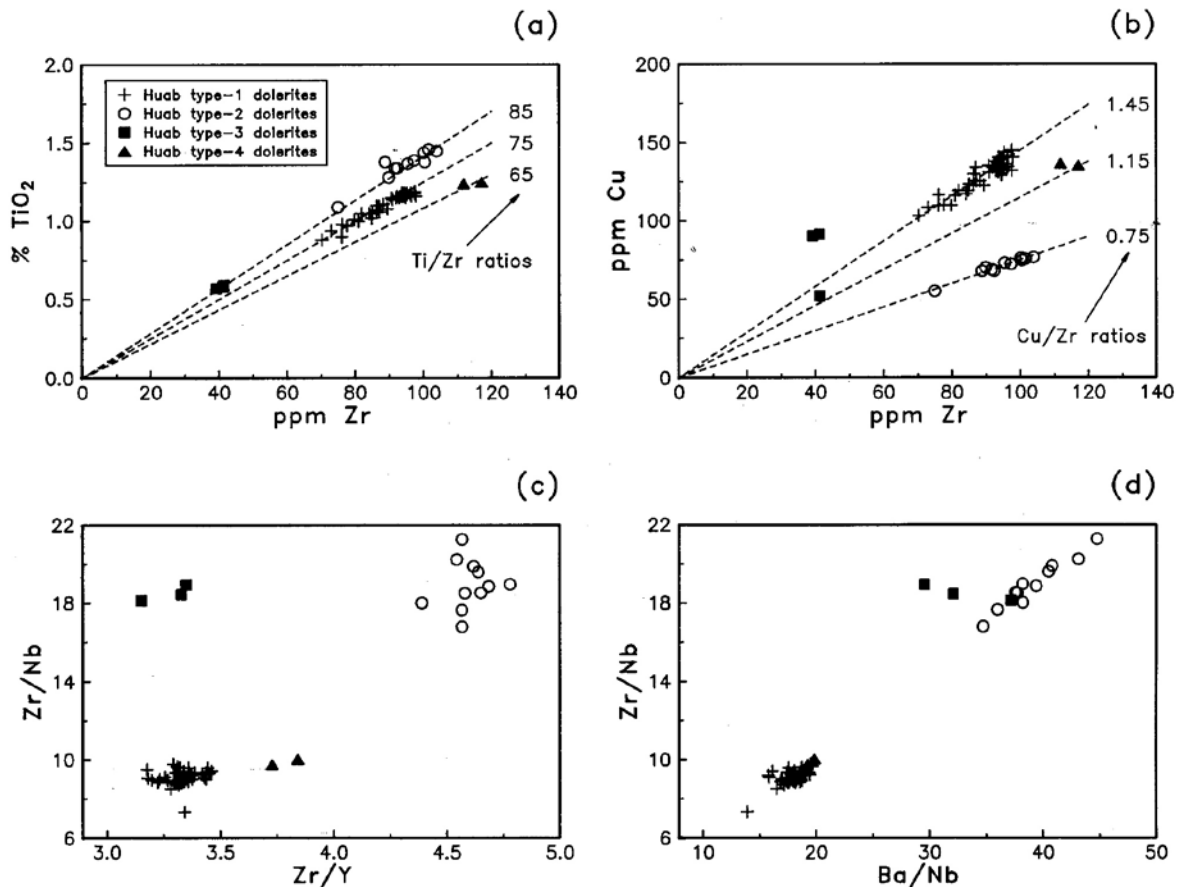


Fig. 2: Plots of compositional data for the Huab dolerites to illustrate the differences in elemental abundances and ratios for selected incompatible elements in the four compositional groups defined in this paper.

ratios of incompatible elements indicate that the dolerite types are not related by fractional crystallisation processes.

The four different compositional groups have been termed type-1, -2, -3 and -4 dolerite with the largest number of samples constituting type-1 and the smallest number of samples type-4. The major sills in the study area are either type-1 or type-2 dolerite with type-3 and type-4 dolerite occurring only as small sills of limited lateral extent. Two dykes in the study area are of type-1 dolerite, whereas the other three dykes sampled do not correspond in composition to any of the dolerite types represented by sills. All five of the analysed dykes intrude Karoo Sequence sediments.

The mean compositions of each of the four dolerite types are given in Table 1. The data given in Table 1 and depicted in various figures in this paper have been recalculated so that the major oxides sum to 100% on a volatile-free basis with all Fe expressed as FeO*.

All the dolerite types are tholeiitic in composition, containing both normative hypersthene and olivine. They are rather primitive in character with relatively high concentrations of MgO, Ni and Cr (see Table 1) and the more magnesian varieties of type-1 dolerite and all type-3 dolerites have Mg numbers (calculated as the

atomic ratio of $Mg/Mg+Fe^{2+}$ with $Fe^{2+}O_3/FeO$ assumed to be 0.2) of approximately 70 which indicates that magmas of this composition could have been in equilibrium with mantle olivine (Kesson, 1973). Fig. 3 illustrates a significant range in Mg number and its smooth covariation with an incompatible element (Ti expressed as TiO_2) and a compatible element (Ni) for both type-1 and type-2 dolerites.

Of the vertical sections which were sampled through the sills at different localities (see Fig. 1), the samples from Sections A, B, D and F are type-1 dolerite and the samples from Section E are type-2 dolerite. The uppermost sample in Section C is a type-1 dolerite, but the remaining samples from Section C are all type-2 dolerite. A thin screen or lens of metamorphosed Karoo sediment occurs just below the uppermost sample in Section C and if this horizon is followed northwards it becomes a persistent metasedimentary band some 1-2 m thick separating two sills with clearly defined chill margins against the sediment. The two sills at this locality were not seen in direct contact with one another and it was not possible to establish the relative order of intrusion of dolerite types 1 and 2. Dolerite type-4 intrudes a type-3 dolerite sill and an early basalt flow of the Etendeka Formation.

TABLE 1: Mean compositions of Huab Valley dolerite types.

| | Type-1 (n=42) | Type-2 (n=11) | Type-3 (n=3) | Type-4 (n=2) |
|--------------------------------|------------------|------------------|-----------------|-----------------|
| SiO ₂ | 48.37 | 49.03 | 50.45 | 50.67 |
| TiO ₂ | 1.11 | 1.36 | .58 | 1.25 |
| Al ₂ O ₃ | 16.66 | 15.66 | 16.39 | 15.54 |
| FeO* | 10.61 | 11.10 | 7.84 | 11.13 |
| MnO | .18 | .18 | .15 | .19 |
| MgO | 8.26 | 8.54 | 9.68 | 7.38 |
| CaO | 11.78 | 10.54 | 12.60 | 10.54 |
| Na ₂ O | 2.35 | 2.92 | 2.08 | 2.29 |
| K ₂ O | .54 | .54 | .18 | .86 |
| P ₂ O ₅ | .13 | .14 | .05 | .16 |
| Rb | 16 | 11 | 3.8 | 29 |
| Ba | 175 | 195 | 72 | 226 |
| Sr | 220 | 329 | 276 | 210 |
| Zr | 90 | 94 | 41 | 115 |
| Nb | 9.9 | 5.0 | 2.2 | 12 |
| Cr | 319 | 324 | 412 | 269 |
| V | 258 | 295 | 177 | 291 |
| Sc | 36 | 25 | 34 | 35 |
| Ni | 156 | 168 | 193 | 141 |
| Co | 56 | 59 | 55 | 54 |
| Zn | 77 | 78 | 54 | 88 |
| Cu | 129 | 71 | 78 | 136 |
| Y | 27 | 20 | 12 | 30 |
| La | 9.7 | 11 | 3.7 | 13 |
| Ce | 22 | 21 | 8.2 | 30 |
| Nd | 14 | 15 | 4.7 | 18 |
| Zr/Nb | 9.09 | 18.8 | 18.6 | 9.58 |
| Zr/Y | 3.33 | 4.70 | 3.42 | 3.83 |
| Ti/Zr | 73.9 | 86.7 | 84.8 | 65.1 |
| Cu/Zr | 1.43 | 0.76 | 1.90 | 1.18 |
| Ba/Nb | 17.7 | 39.0 | 32.7 | 18.8 |

Note: Data for U, Th and Pb have been omitted from this table as their concentrations were below detection limit (< 2.5 ppm) in many of the samples analysed.

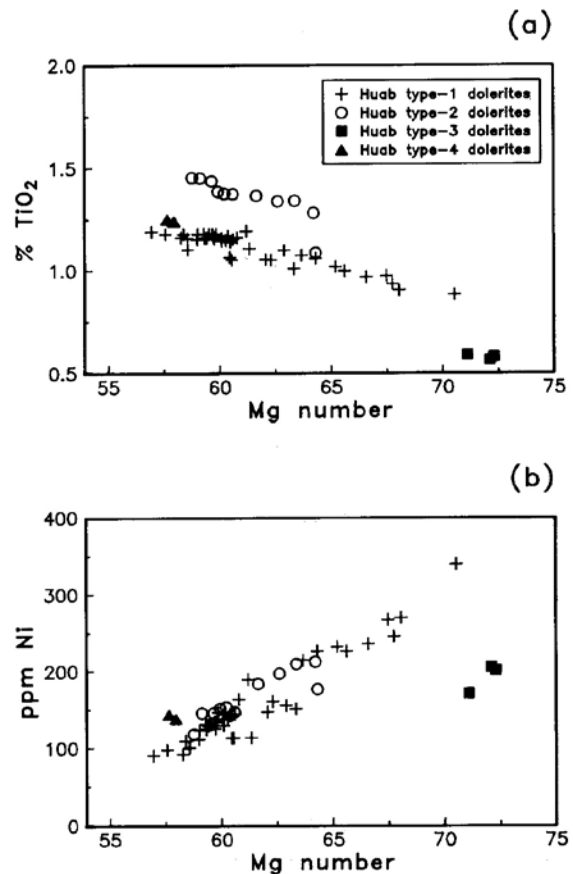


Fig. 3: Compositional variations within the Huab dolerite types as shown by the co-variation of (a) an incompatible element (Ti expressed as TiO_2) with Mg number (the atomic ratio of $Mg/Mg+Fe^{2+}$ with Fe_2O_3/FeO assumed to be 0.2); and (b) a compatible element (Ni) with Mg number.

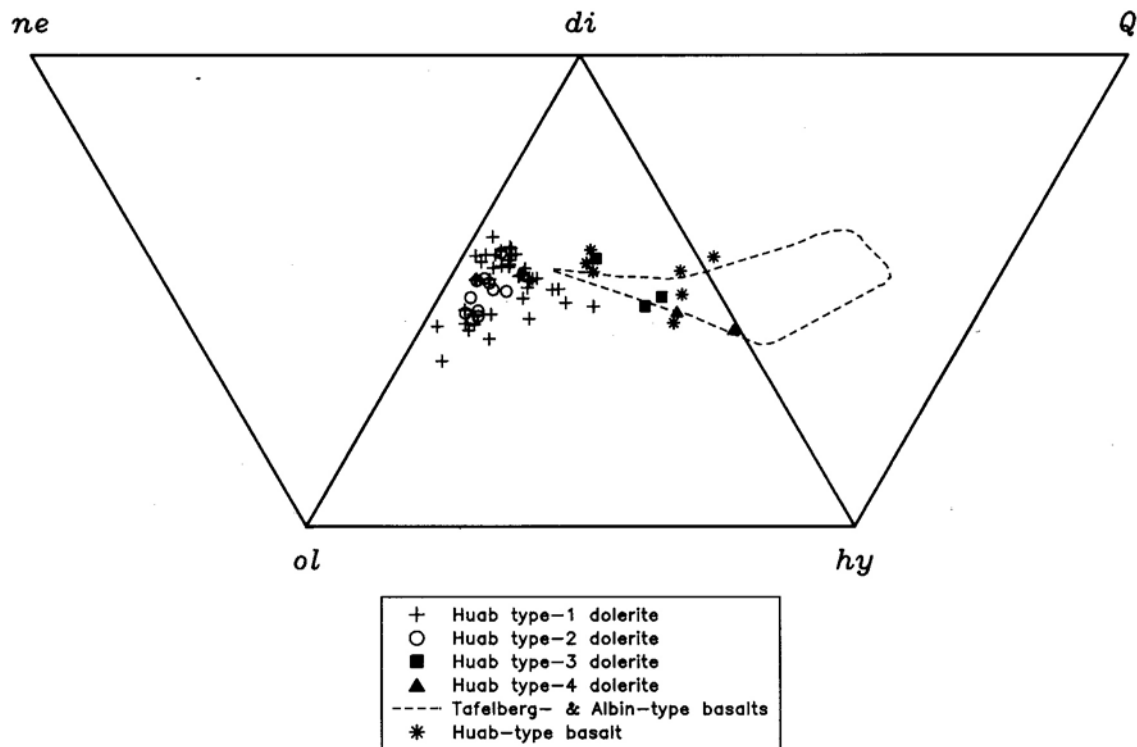


Fig. 4: Basalt quadrilateral diagram (normative Q - di - ne - ol - hy) for the Huab dolerites and low- TiO_2 basalts of the Etendeka Formation. The CIPW normative data on which this diagram is based were calculated with Fe_2O_3/FeO assumed to be 0.2. The dashed line encloses the field occupied by data points for 122 Tafelberg- and Albin-type basalts.

Comparison with Etendeka Formation basalts

When comparing the Huab dolerites with Etendeka Formation basalts it is only appropriate to compare them with the low- TiO_2 basalts (containing $< 2.5\%$ TiO_2) which consist of the Tafelberg and Albin-type basalts (Erlank *et al.*, 1984) and the Huab-type basalts (Duncan *et al.*, 1988). The high- TiO_2 basalts which have been termed the Khumib-type basalts (Duncan, 1987; Duncan *et al.*, 1988) are clearly of quite different composition from any dolerite discussed in this paper.

The most striking difference between the Huab dolerites and the basaltic lavas of the Etendeka Formation is that the type-1 and type-2 dolerites are more basic than the lavas. This is particularly well illustrated by the basalt quadrilateral (Fig. 4) where the data for these dolerites plot in a field distinct from that occupied by the basalts, due to a higher proportion of normative olivine and less normative hypersthene. It is also indicated by the generally higher MgO (Fig. 5b) and lower Zr (Fig. 5a) concentration in the dolerites compared to those in the Tafelberg- and Albin-type basalts.

The Huab-type basalts could be considered a more basic variant of the Tafelberg-type but for their distinctly higher ϵNd values (Duncan *et al.*, 1988; Fig. 3). They are a very minor basalt variety in terms of abundance, but are found within a large area comprising the main Etendeka lava field and many of the smaller lava remnants south of latitude $18^{\circ}30'S$. The Huab-type ba-

salts are the basalt variety which is most similar to the Huab dolerites, but they contain less normative olivine (Fig. 4), and a lower concentration of TiO_2 at comparable MgO concentrations (Fig. 5b), than almost all the dolerites.

The compositional relationships shown in Fig. 5 also suggest that only the Huab type-3 dolerites could be related by low-pressure fractional crystallisation to the Tafelberg, Albin or Huab-type basalts of the Etendeka Formation. On the basis of the compositional data one must therefore conclude that the voluminous and widespread dolerites in the Huab valley (type-1 and -2 dolerites) do not represent subvolcanic equivalents of the Etendeka Formation basalts.

Comparison with other dolerites in the Etendeka area

The most common dolerite varieties intruding the volcanic rocks of the Etendeka Formation are those which are compositionally equivalent to the Tafelberg-type basalts and texturally very similar to either the Tafelberg or Albin-type basalts (Erlank *et al.*, 1984). These dolerites are not compared with the Huab dolerites as they are identical in composition to the Tafelberg-type basalts which were discussed in the previous section.

Additional dolerite types which are associated either spatially and/or temporally with the Etendeka Formation are the Horingbaai dolerites, some ophitic-textured dolerites which are compositionally similar to the Tafel-

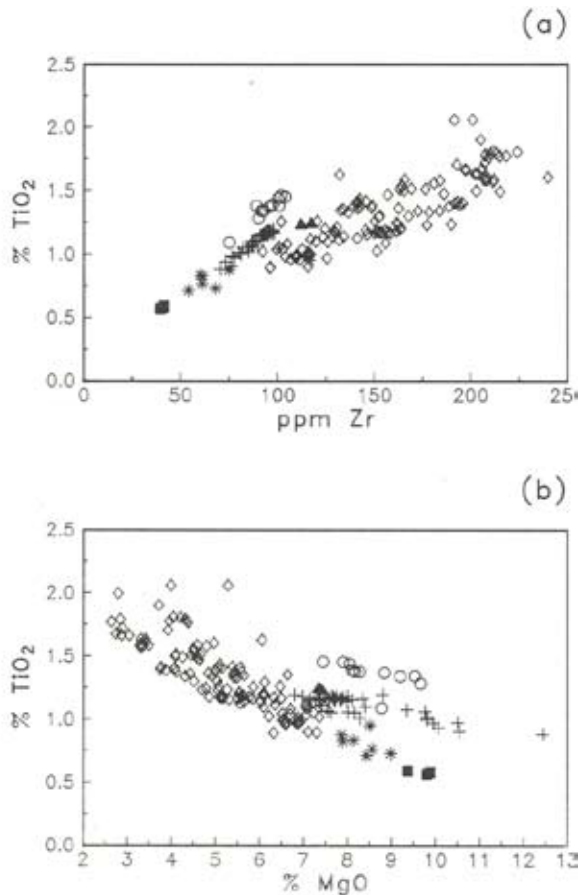


Fig. 5: Some compositional comparisons between Huab dolerite types and the low-TiO₂ basalts of the Etendeka Formation. In particular, note the different TiO₂ concentrations at similar MgO values in the Huab type-1, -2 and -4 dolerites compared to the basalts, and the relatively higher Ti/Zr ratios of the same three dolerite types. Symbols are the same as in Fig. 4, with open diamond symbols denoting low-TiO₂ Etendeka basalts.

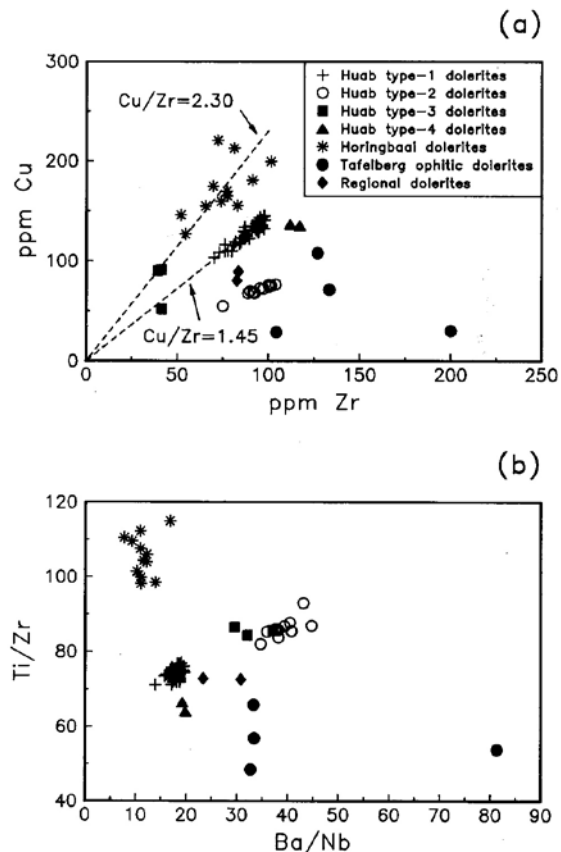


Fig. 6: Compositional comparisons between Huab dolerite types and some other dolerites associated with the Etendeka Formation.

have continued to denote them as regional dolerites in Fig. 6. They are compositionally very similar to the Huab dolerites in the present study area, but do not appear to be identical to any of the four types defined in this study (see Fig. 6).

Petrography and mineral chemistry

berg-type basalts, and “regional dolerites” intruding the Karoo sediments. All three of these dolerite varieties were defined and discussed by Erlank *et al.*, (1984).

The Horingbaai dolerites have MORB affinities with flat REE patterns and isotopic data which plot within the “mantle array” in the depleted quadrant of an ϵSr vs. ϵNd diagram (Hawkesworth *et al.*, 1984; Fig. 4). They are broadly similar in composition to the Huab dolerites but can be distinguished from them by their higher Cu/Zr and Ti/Zr ratios (see Fig. 6).

Ophitic-textured Tafelberg dolerites are very variable in composition, making it difficult to compare them meaningfully with the Huab dolerites. However, the data suggest that they have generally lower Cu/Zr and Ti/Zr ratios than the Huab dolerites (Fig. 6).

The two samples described as “regional dolerites” by Erlank *et al.*, (1984) were collected from a sill which intrudes Karoo sediments near the mouth of the Huab River (west of the present study area) and geographically must be considered as part of the Huab dolerite suite. However, to facilitate compositional comparison between these samples and those in the study area we

Huab type-1 and type-2 dolerites can not be distinguished from each other petrographically. The coarse-grained varieties found near the centre of a sill have ophitic or sub-ophitic textures with large clinopyroxene oikocrysts (up to 10 mm in maximum dimension), euhedral plagioclase chadocrysts (up to 2 mm long) and intergranular olivine (up to 3 mm in maximum dimension). Accessory phases are titanomagnetite, ilmenite, chrome-spinel, pyrite and apatite. Finer-grained varieties near the margins of the sills have intergranular or sub-ophitic textures. Samples taken within a few centimetres of the chilled margin of a sill are porphyritic with phenocrysts of plagioclase and olivine set in a relatively coarse intergranular groundmass. Phase proportions in the central portion of a sill are typically 45% plagioclase, 35-40% clinopyroxene, 10-15% olivine and about 5% accessory phases.

Type-3 dolerites are petrographically distinctive with very well developed ophitic textures but with much

smaller plagioclase chadocrysts than in type-1 or type-2 dolerites. The well-developed ophitic texture is responsible for the mottled appearance of hand specimens of this dolerite type. Modal proportions are typically 50% clinopyroxene, 40% plagioclase, 5-10% olivine and about 2% accessory phases (mainly opaque oxides).

The two type A dolerite samples are both intergranular textured and could not be distinguished by texture or modal proportions from type-1 or type-2 dolerites sampled near a sill margin.

The variation of MgO content with height in the six vertical sections sampled through the sills is shown in Fig. 7. Sections D and F show marked increases in MgO content in the lower portion of the sill, while Section E shows an increase in MgO in the central portion of the sill. The samples that were chosen for microprobe analysis were mainly selected from Sections D, E and F so that the mineral chemistry obtained could be used for quantitative petrogenetic modelling (see Fig. 7 for

sample locations within these sections). One sample of a type-3 dolerite (KLS-506) was also selected for microprobe analysis.

Pyroxene and olivine compositions in the analysed samples are shown in Fig. 8. The compositional range is from $WO_{45}En_{45}Fs_{10}$ to $WO_{40}En_{30}Fs_{30}$. The Wo component shows little variation in individual pyroxene oikocrysts and no systematic trend. This is in contrast to the Fs component which increases in the Fe-rich rims which are a common feature of the larger oikocrysts. The typical range observed is Fs_{10-19} and it is only in sample KLS-524 that very Fe-rich pyroxene rims (Fs_{30}) are observed. The absence of pigeonite in any of the Huab dolerites is notable since this is a common phase in many Karoo dolerites. The olivine compositional range is Fo_{83-41} . Individual olivine crystals show great variations in the degree of compositional zonation. Some are almost unzoned ($Fo_{66.4-65.7}$), whereas others are very strongly zoned ($Fo_{66.7-48.5}$). In all cases the zonation

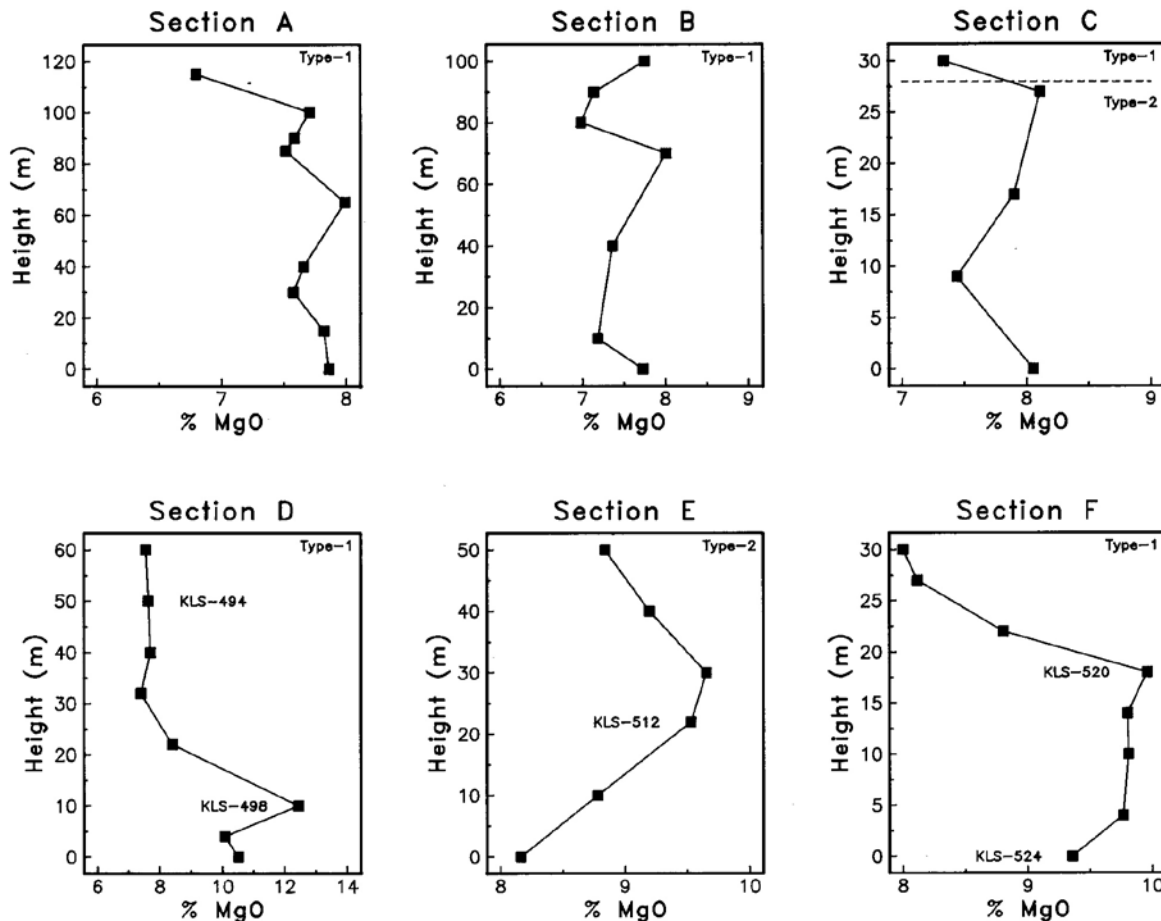


Fig. 7: Compositional variation with sample height in six sections through dolerite sills in the Huab valley (localities are shown in Fig. 1). Heights are expressed relative to the lowest sample in each section and *not* relative to the base of the sill since the base is not exposed in 4 of the 6 sections. In Section A the top contact has been eroded, the lower contact with Prince Albert Formation marls is 1-2 m below the lowest sample. In Section B the top sample is approximately 2-3 m below the contact with Etjo sandstone, the lower contact of Section C is not exposed. The relationship between Sections B and C is discussed in the text. In Section D the top contact has been eroded and the lower contact is not exposed. In Section E the top sample is approximately 5 m below the contact with Etjo sandstone, the lower contact is not exposed. In Section F the top sample is approximately 1 m below the contact with Damara schists and the bottom sample is approximately 1 m above the lower contact with Damara schists. The sample numbers shown are for samples in which mineral compositions were determined.

is "normal" with the crystal rims being more Fe-rich.

In basic rocks the Mg/Fe ratio of olivine is generally higher than that of the co-existing clinopyroxene. Examination of Fig. 8 shows that this relationship is true for olivine and augite in sample KLS-524, but not for the other samples analysed. The olivines in all samples other than KLS-524 are also much more Fe-rich than predicted by the Roeder and Emslie (1970) Fe/Mg par-

titution coefficient, assuming the sample composition to be that of a liquid with an $\text{Fe}^{2+}/\text{FeO}$ ratio of 0.2. In the following list the most magnesian olivine composition analysed in each sample is given together with the calculated equilibrium olivine based on the assumptions just noted given in parentheses: KLS-494 - Fo_{67} (Fo_{84}), KLS-498 - Fo_{73} (Fo_{89}), KLS-520 - Fo_{75} (Fo_{87}), KLS-524 - Fo_{83} (Fo_{86}), KLS-512 - Fo_{63} (Fo_{85}). The general difference between measured and calculated olivine compositions could be due in part to some or all of the samples being enriched in cumulus olivine, but the differences are so large in some samples that this cannot be the only explanation.

The most probable explanation for the relatively Fe-rich olivine compositions in samples in the interior of the sills is re-equilibration of early-crystallised magnesian olivine with residual liquid during the later stages of crystallisation. This explanation was also suggested by Richardson (1979) for olivines in the Tandjesberg sill in southern Namibia and by Erlank *et al.*, (1984) for some of the dolerites in the Etendeka Formation. The latter authors also noted that if this process was operative then the coexistence of Fe-rich olivine with Mg-rich clinopyroxene must be attributed to radically different kinetics for Fe-Mg partitioning between olivine-liquid and pyroxene-liquid. Erlank *et al.*, (1984) also suggested that magma mixing might be an explanation for apparent compositional disequilibrium between olivine and pyroxene. There is no evidence in the Huab sills of strongly bimodal compositions in a single mineral species and it thus seems unlikely that mixing of magmas with different compositions has been a major process in their genesis.

The compositions of plagioclase in the type-1 dolerites from Sections D and F show a range of An_{87-41} . There are slight differences in the total range of plagioclase compositions in different samples but no marked differences between different samples. Plagioclase in sample KLS-512 from Section E is slightly less calcic with a range of An_{77-38} . Sample KLS-520 is unique amongst those analysed by electron microprobe in having alkali feldspar (Or_{45-32}) as rims on several large plagioclase crystals and as small intergranular crystals.

The opaque minerals analysed in the selected samples not only show significant compositional differences in specific mineral species in different samples, but also show quite different assemblages of opaque minerals in different samples. For instance, sample KLS-524 contains chromspinel and titanomagnetite but no ilmenite, whereas KLS-520 from near the centre of the same sill contains ilmenite as the only oxide phase. The general case is that samples from near the centre of a sill are more ilmenite-rich and titanomagnetite-poor than those near the chill margins, presumably reflecting the relative cooling rates and oxygen fugacities of the immediate environment. Sample KLS-512 from Section E contains titanomagnetite with trellis-type ex solution of ilmenite. Using the data of Buddington and Lindsley

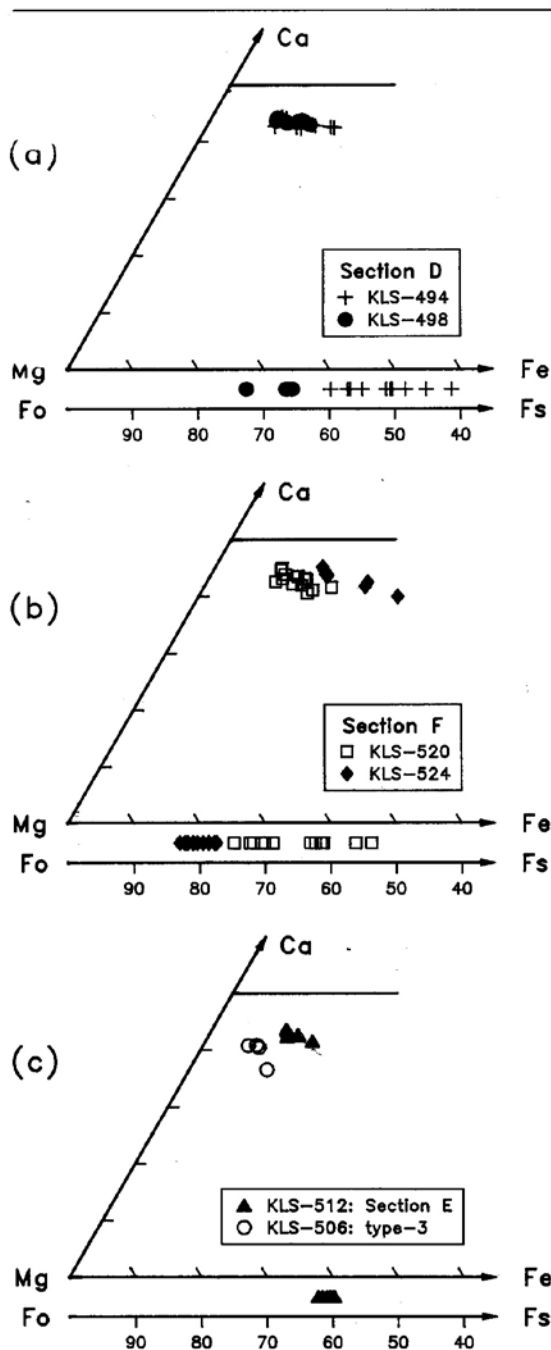


Fig. 8: Pyroxene and olivine compositions in selected samples of the Huab dolerites. The relative positions of analysed samples from Sections D, E and F are shown on Fig. 7 (a) samples from Section D; (b) samples from Section F; (c) sample from Section E and the one type-3 dolerite in which minerals were analysed (KLS-506). Note that olivine occurs in KLS-506 but is too altered for microprobe analysis.

(1964) the calculated equilibration temperature of these phases is approximately 690°C (sub-solidus) and the oxygen fugacity is between the FMQ and NNO buffer curves.

Petrogenetic modelling

Variations in the MgO content with height in the six vertical sections through the sills are illustrated in Fig. 7 and were discussed briefly in the previous section. Section D shows the largest range in MgO content, while the variations in another major oxide (CaO) and five trace elements (Ba, Zr, Ni, Co and V) as a function of stratigraphic height in this section are shown in Fig. 9. Comparison of Figs 7 and 9 shows sympathetic relative enrichments in MgO, Ni and Co, and relative depletions in CaO, Ba, Zr and V in the lower portion of the sill. These complementary variations in composition are qualitatively consistent with phenocryst enrichment, particularly of olivine, in the lower portion of the sill. Samples from Section F show similar complementary variations in composition (Fig. 10) but the proportion of the sill showing relative enrichment in MgO, Ni and Co is much greater than in Section D. The elements Zr and

Ba can be considered as incompatible elements during the main phase of crystallisation of the Huab dolerites since they are not significantly partitioned into any of the main phases crystallising (olivine, plagioclase and augite). The lowest concentrations of Zr and Ba in Figs 9 and 10 can thus be interpreted as markers for the zone of maximum phenocryst accumulation. The highest concentration of these elements may indicate the last portion of the sill to crystallise, but will not necessarily do so if the process by which phenocrysts are concentrated is one of flow age differentiation (Bhattacharji and Smith, 1967).

A common application of quantitative petrogenetic modelling techniques is to simulate the derivation of successive magmatic *liquids* from a parental magma by one or more processes such as crystal fractionation, wall-rock assimilation or magma mixing. If we are to use quantitative modelling techniques for samples from a single sill then we must be alert to the possibility that some samples will not represent magmatic liquids. Indeed, if the conclusions of the previous paragraph are valid, then samples with the lowest concentrations of Ba and Zr are likely to be cumulus enriched in one or more phases.

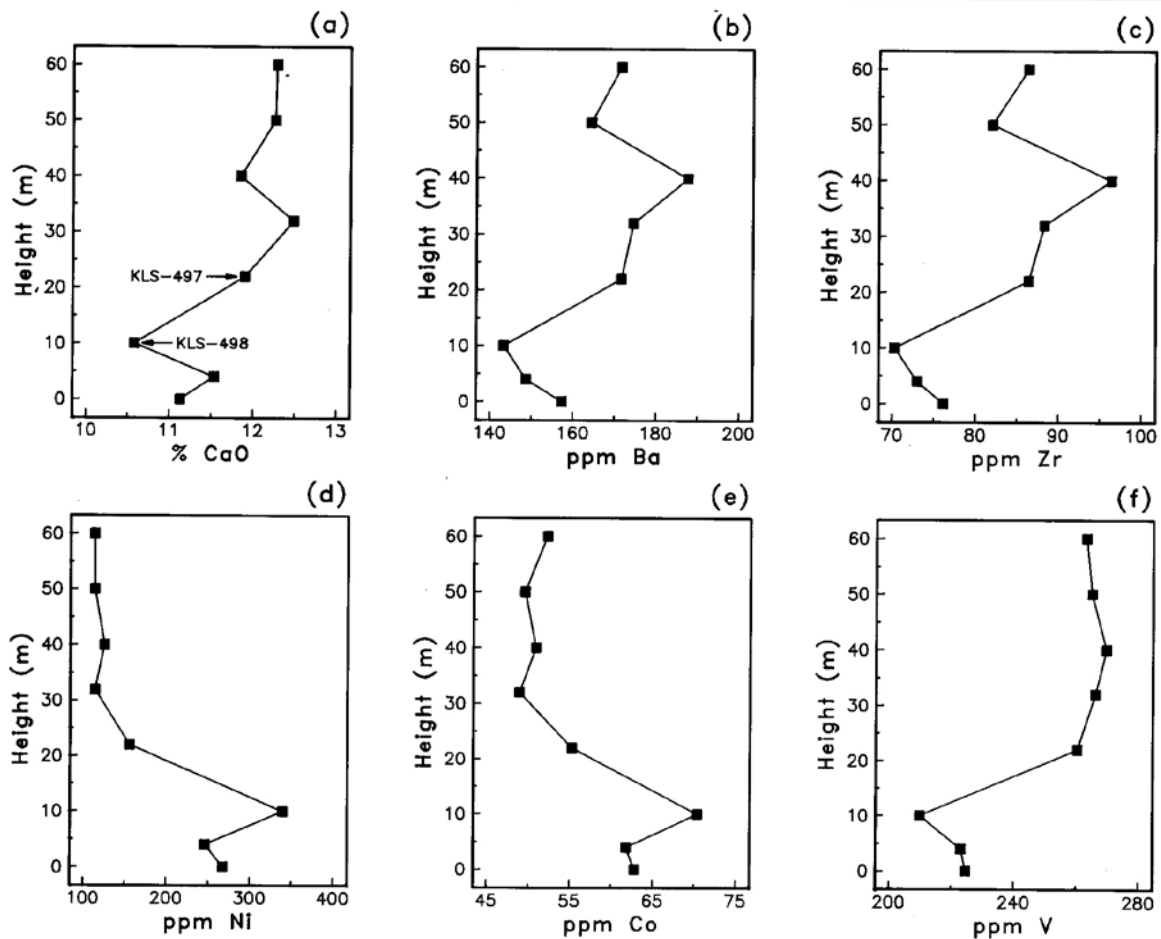


Fig. 9: Compositional variation with sample height in Section D through a dolerite sill in the Huab Valley (see Fig. 1 for locality). A quantitative model to generate sample KLS-498 by cumulus phase addition to sample KLS-497 is discussed in the text and presented in Table 2.

The aim of our model calculations is to establish whether the compositional variations within a sill can be quantitatively attributed to phenocryst enrichment in some sections of the sill and to relative removal of phenocrysts from other sections. As far as the modelling is concerned we can treat both possibilities as crystal fractionation processes and it is not necessary to distinguish between different physical mechanisms (e.g. gravitational separation or flow age differentiation) by which the fractionation takes place. The quantitative techniques for modelling phenocryst enrichment and phenocryst removal are somewhat different and examples of each are given in the following two sections of this paper.

Modelling a partial cumulate in Section D

Neither the upper nor lower contact of the sill is exposed in Section D, although the relatively fine-grained character of the lowest sample suggests that it is not far above the base. Without any sample at or close to a chill margin, and without samples representing a complete section through the sill, it is not possible to estimate the original composition of the intruding magma. We have therefore chosen to model the sample with the lowest Zr content (KLS-498) by a process of cumulus enrichment into a magma with the composition of the next sample above it (KLS-497) in the section (see Fig. 9a for the relative positions of these samples within Section D). For a model of this type it does not matter if KLS-497 is itself cumulus enriched in some phases rather than a true magmatic liquid.

The major elements in KLS-498 have been modelled using a least squares linear mixing technique as implemented in the GENMIX computer program (Le Maitre, 1981). Input data for the models were major oxides recalculated to 100% totals with all Fe expressed as FeO (shown as FeO*) in the two rock compositions and in the analysed mineral phases whose compositions were discussed in the previous section of this paper. Satisfactory models with low values for the sum of squares of the differences between the calculated oxide abundances and those actually measured in KLS-498 could only be obtained if rather magnesian olivine (Fo_{82}) and calcic plagioclase (An_{86}) were used as the cumulus phases to be added to KLS-497. The olivine composition is more magnesian than that found in KLS-498 (Fig. 8) but is slightly less magnesian than the calculated equilibrium olivine (Fo_{85} - Roeder and Emslie, 1970) in KLS-497. This is in accord with the suggestion made earlier in this paper that the relatively Fe-rich olivine compositions analysed in many samples may reflect re-equilibration processes. It was not possible to obtain satisfactory models if augite of any of the analysed compositions was included in the cumulus phase assemblage, suggesting that it was not a liquidus phase in this sill when KLS-498 was formed. Inclusion of small amounts of titanomagnetite in the cumulus assemblage slightly im-

TABLE 2: Quantitative model to derive KLS-498 by phenocryst enrichment into a magma of KLS-497 composition. See Fig. 9a for the relative positions of these two samples within Section D.

| | Input Data | | | Model | | |
|--------------------------------|------------|---------|-------|---------|--------------------|------|
| | KLS-497 | Olivine | Plag. | KLS-498 | Component | % |
| SiO ₂ | 48.21 | 38.77 | 47.56 | 46.86 | KLS-497 Olivine | 80.7 |
| TiO ₂ | 1.10 | 0.00 | 0.00 | 0.88 | | 13.2 |
| Al ₂ O ₃ | 16.90 | 0.07 | 32.85 | 15.80 | Plag. | 6.1 |
| FeO* | 10.25 | 17.11 | 0.44 | 10.74 | | |
| MnO | 0.17 | 0.25 | 0.00 | 0.18 | | |
| MgO | 8.41 | 43.25 | 0.15 | 12.45 | | |
| CaO | 11.90 | 0.38 | 17.44 | 10.58 | | |
| Na ₂ O | 2.43 | 0.00 | 1.54 | 1.99 | | |
| K ₂ O | 0.49 | 0.00 | 0.07 | 0.42 | | |
| P ₂ O ₅ | 0.13 | 0.00 | 0.00 | 0.11 | | |

| Partial Cumulate Model for KLS-498 | | | | | | | |
|------------------------------------|----------------|-------|-------|---------|---------|-------|-----|
| | Major Elements | | | KLS-497 | KLS-498 | Model | |
| | KLS-498 | Model | Diff. | | | | |
| SiO ₂ | 46.86 | 46.93 | 0.07 | Rb | 13 | 12 | 11 |
| TiO ₂ | 0.88 | 0.89 | 0.01 | Ba | 171 | 142 | 141 |
| Al ₂ O ₃ | 15.80 | 15.66 | -0.14 | Sr | 224 | 207 | 205 |
| FeO* | 10.74 | 10.55 | -0.19 | Zr | 86 | 70 | 70 |
| MnO | 0.18 | 0.17 | -0.01 | Nb | 9.2 | 7.6 | 7.7 |
| MgO | 12.45 | 12.49 | 0.04 | Cr | 344 | 507 | 409 |
| CaO | 10.58 | 10.72 | 0.14 | V | 259 | 208 | 214 |
| Na ₂ O | 1.99 | 2.06 | 0.07 | Sc | 35 | 29 | 29 |
| K ₂ O | 0.42 | 0.40 | -0.02 | Ni | 155 | 337 | 316 |
| P ₂ O ₅ | 0.11 | 0.11 | 0.00 | Co | 55 | 70 | 71 |
| | | | | Zn | 73 | 76 | 76 |
| | | | | Cu | 129 | 103 | 105 |
| | | | | Y | 26 | 21 | 21 |
| | | | | La | 7.1 | 5.1 | 5.9 |
| | | | | Ce | 19 | 13 | 15 |
| | | | | Nd | 13 | 9 | 11 |

Sum of squares of major element differences = 0.09

proved the calculated major element models but is not compatible with the trace element modelling (see below) and appears on textural grounds to be a late-crystallising phase. The most satisfactory major element model is shown in Table 2.

For modelling trace elements in a crystal accumulation process the equation of Gast (1968) as modified by Le Roex and Reid (1978) has been used. This is:

$$C_a/C_a^o = (1-F^D)/(1-F)$$

where:

C_a = average concentration of element a in a suite of perfectly zoned minerals.

C_a^o = concentration of element a in the original liquid.

F = weight fraction of liquid remaining.

D = bulk distribution coefficient for element a.

Le Roex and Reid (1978) note that two assumptions are necessary before crystal accumulation can be quantitatively modelled. These are: (1) that phenocrysts were homogeneously distributed throughout the magma; and (2) that at the instant when the weight fraction of liquid remaining was equal to a particular value of F, all the

TABLE 3: Trace element distribution coefficients used in petrogenetic modelling.

| | Mineral Phases | | | |
|----|----------------|-------------|--------|-----------|
| | Olivine | Plagioclase | Augite | Magnetite |
| Rb | .05 | .05 | .06 | (.01) |
| Ba | .0001 | .3 | .002 | (.01) |
| Sr | .07 | 1.6 | .08 | (.01) |
| Zr | .04 | .06 | .6 | .1 |
| Nb | .15 | .1 | .05 | .4 |
| Cr | 3 | .02 | 5 | 50 |
| V | .14 | .01 | 1.8 | 25 |
| Sc | .22 | .01 | 3.2 | 1.0 |
| Ni | ** | .05 | 2.8 | 1.4 |
| Co | 3.8 | .02 | 1.2 | 3.4 |
| Zn | 1.8 | .1 | .5 | 12 |
| Cu | .02 | .05 | .07 | 5 |
| Y | .01 | .1 | .42 | .2 |
| La | .0002 | .07 | .069 | (.01) |
| Ce | .0005 | .10 | .098 | (.01) |
| Nd | .0010 | .18 | .180 | (.01) |

Notes: Ni distribution coefficients were (**) calculated from the MgO content of the parent magma using the formula of Smith *et al.* (1980). The value for the model shown in Table 2 is 11.6 and for the model shown in Table 4 is 10.2.

Values shown in parentheses are estimated distribution coefficients. Sources of data: Leeman and Scheidegger (1977); Ross (1977); Paster *et al.* (1974); Philpotts and Schmetzler (1970); Griffin and Rama Murthy (1979); Dale and Henderson (1972); Hakli and Wright (1967); Bougault and Hekinian (1974); Gorton (1974); Dupuy and Coulon (1973); Irving (1978); Leeman *et al.* (1978); Pearce and Norry (1979); Cox *et al.* (1984).

phenocrysts migrated to the cumulus-enriched zone. These assumptions enable an estimate for the maximum value of F, using the equation:

$$F = 1 - M(V_1/V_2)$$

where:

M = weight fraction of phenocrysts added to the cumulus enriched zone.

V₁ = volume of the cumulus enriched zone.

V₂ = volume of magma from which the phenocrysts were derived.

The ratio V₁/V₂ may be replaced by the ratio of the respective thicknesses D₁/D₂ if it is assumed that the direction of phenocryst migration was predominantly vertical, thus:

$$F = 1 - M(D_1/D_2)$$

The values of D₁ and D₂ have been estimated from Fig.

9 (D₁ = 15 m, D₂ = 45 m) and the value for M of 0.193 was obtained from the major element mixing model. This gives a value of F = 0.936 which was used to calculate the concentration of each element in the cumulus phases using the distribution coefficients given in Table 3. The concentration of each element in the cumulus enriched zone (as represented by sample KLS-498), designated C_a^o, was calculated using the equation:

$$C_a^o = C_a^i(1-M) + C_a^m M$$

The values obtained are given in Table 2, where they are compared with the analysed concentrations in KLS-498.

The overall major and trace element model presented in Table 2 is satisfactory in terms of the generally excellent agreement between the calculated values for each element and the observed values in KLS-498. It is important to note that agreement is obtained both for incompatible trace elements (such as Ba, Zr and Nb) and compatible elements (such as Sr, Ni, Co and Zn). The largest discrepancy is for Cr and this could be corrected by including a minute amount of Cr-spinel, which is an early-crystallising phase in the Huab dolerites, in the model.

Note that the model value for V is slightly higher than the observed concentration in KLS-498. This provides a constraint against including titanomagnetite in the cumulus phase assemblage due to its very high distribution coefficient (25 - see Table 3) which would result in any partial cumulate model including this phase having a much higher V value than that observed in KLS-498.

TABLE 4: Quantitative model to derive KLS-519 by crystal fractionation from a magma of KLS-524 composition. See Fig. 10a for the relative positions of these two samples within Section F.

| | Input Data | | | Model | | | |
|--|----------------|-------|-------|----------------|-----------|-------|------|
| | KLS-524 | Oliv. | Plag. | KLS-519 | Component | % | |
| SiO ₂ | 48.32 | 38.77 | 50.16 | 50.98 | Augite | 67.3 | |
| TiO ₂ | 1.08 | 0.00 | 0.00 | 0.79 | Plag. | 24.1 | |
| Al ₂ O ₃ | 16.02 | 0.07 | 31.11 | 3.28 | Olivine | 8.6 | |
| FeO* | 11.03 | 17.11 | 0.40 | 7.01 | F = | 0.906 | |
| MnO | 0.19 | 0.25 | 0.00 | 0.16 | | | |
| MgO | 9.36 | 43.25 | 0.24 | 15.70 | | | |
| CaO | 11.13 | 0.38 | 15.29 | 21.34 | | | |
| Na ₂ O | 2.19 | 0.00 | 2.69 | 0.31 | | | |
| K ₂ O | 0.57 | 0.00 | 0.11 | 0.01 | | | |
| P ₂ O ₅ | 0.13 | 0.00 | 0.00 | 0.00 | | | |
| Derivative liquid model for KLS-519 | | | | | | | |
| | Major Elements | | | Trace Elements | | | |
| | KLS-498 | Model | Diff. | KLS-497 | KLS-498 | Model | |
| SiO ₂ | 47.92 | 48.17 | 0.25 | Rb | 20 | 19 | 22 |
| TiO ₂ | 1.19 | 1.14 | -0.05 | Ba | 167 | 196 | 183 |
| Al ₂ O ₃ | 16.66 | 16.68 | 0.02 | Sr | 206 | 218 | 218 |
| FeO* | 11.53 | 11.52 | -0.01 | Zr | 90 | 98 | 95 |
| MnO | 0.19 | 0.20 | 0.01 | Nb | 9.6 | 10.9 | 10.6 |
| MgO | 8.80 | 8.84 | 0.04 | Cr | 373 | 161 | 287 |
| CaO | 10.50 | 10.41 | -0.09 | V | 260 | 250 | 255 |
| Na ₂ O | 2.43 | 2.33 | -0.10 | Sc | 36 | 30 | 32 |
| K ₂ O | 0.62 | 0.63 | 0.01 | Ni | 215 | 190 | 180 |
| P ₂ O ₅ | 0.15 | 0.14 | -0.01 | Co | 63 | 61 | 62 |
| | | | | Zn | 81 | 86 | 85 |
| | | | | Cu | 123 | 145 | 135 |
| | | | | Y | 26 | 28 | 28 |
| | | | | La | 8.6 | 9.2 | 9.4 |
| | | | | Ce | 26 | 26 | 28 |
| | | | | Nd | 16 | 16 | 18 |
| Sum of squares of major element differences = 0.08 | | | | | | | |

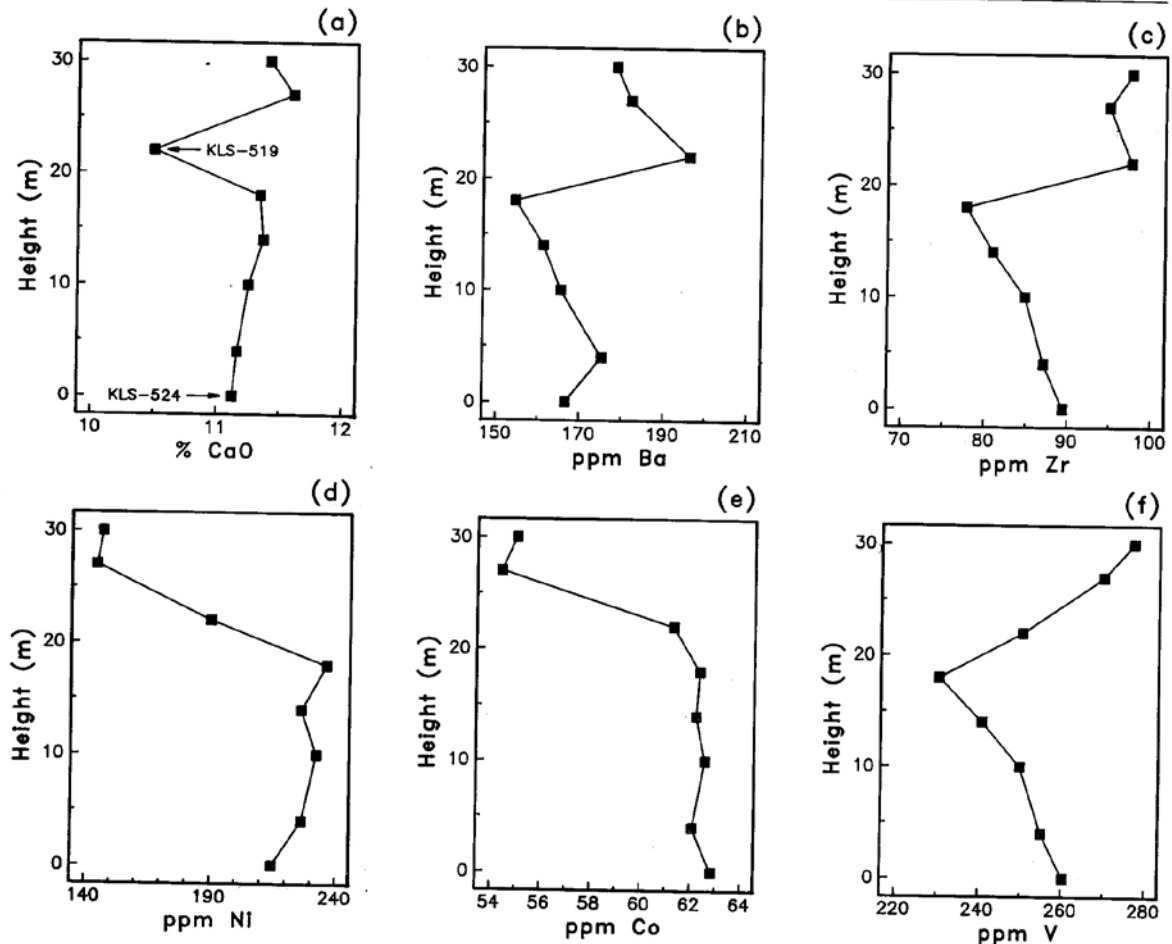


Fig. 10: Compositional variation with sample height in Section F through a dolerite sill in the Huab Valley (see Fig. 1 for locality). A quantitative model for crystal fractionation to generate sample KLS-519 as a derivative liquid from sample KLS-524 is discussed in the text and presented in Table 4.

Modelling a derivative liquid in Section F

The lowermost sample in Section F (KLS- 524) is within 1 m of the lower contact of the sill and is relatively fine-grained. For the purposes of this model we treat KLS-524 as representative of the initial magma composition that was intruded, and have chosen to model the sample with the highest Zr and Ba contents (KLS-519) as a derivative liquid produced by crystal fractionation. The relative locations of these two samples within Section F are shown in Fig. 10a.

A satisfactory major element model once again requires relatively magnesian olivine and augite and a calcic plagioclase, but in this case the phase compositions used are those analysed in KLS-524. No satisfactory major element models could be generated without augite as a fractionating phase and in Table 4 it can be seen that the final model selected has augite and plagioclase as the dominant fractionating phases with olivine as a minor fractionating phase.

The trace elements were modelled using the Rayleigh fractionation equation given by Greenland (1970) which is:

$$C_1/C_0 = F^{D-1}$$

where:

C_1 = concentration of an element in the residual liquid.

C_0 = initial concentration of an element in the original magma.

F = fraction of liquid remaining.

D = bulk distribution coefficient for the element under consideration.

The overall major and trace element model is presented in Table 4. The major element model is generally satisfactory but the difference in SiO_2 content between the model and KLS-519 is rather large (0.25%). The model is satisfactory for compatible elements such as Sr, Sc, Ni and Co but is not satisfactory for Cr. Once again it suggests that small amounts of Cr-spinel may be in the fractionating phase assemblage. The model concentrations of incompatible elements such as Ba, Zr and Nb are slightly lower than those in KLS-519 which suggests that the value of F obtained from the major element model may be slightly lower than that required for an optimum trace element model. The overall model is satisfactory, but is not quite as good as that presented in Table 2 and discussed in the previous section.

The most striking difference between the two models

is the large amount of augite fractionated in this derivative liquid model (67% of the fractionating phase assemblage) compared to its total absence from the partial cumulate model for KLS-598. It should also be noted that olivine and plagioclase are phenocryst phases in KLS-524 but augite is not. We suggest that the explanation for these observations is that KLS-519 represents a derivative liquid separated, at least in part, by filter pressing or flow age differentiation with separation of the liquid from a crystal mush in which the augite oikocrysts (a prominent textural feature in the main portion of the sills) had already crystallised to a significant extent. This is a more complex process than simple crystal fractionation since there is a much higher possibility of crystal-liquid re-equilibration taking place which would not be consistent with the use of the Rayleigh fractionation equation for trace element modelling. This may be an explanation for some of the minor discrepancies noted above and illustrated in Table 4.

Mechanisms of crystal fractionation

The quantitative models discussed above are consistent with the compositional variations observed within a sill being due to addition or removal of phases crystallising from the dolerite magma. In the case of Section D (Fig. 9) the zone of implied crystal accumulation occupies the lower portion of the sill and is a maximum of 30% of the total sill thickness. The model shown in Table 2 suggests that the cumulus assemblage includes only those phases (olivine and plagioclase) which are observed as phenocrysts in the chill margins of the Huab sills. The observations and model are consistent with the mechanism of crystal fractionation in Section D being one of gravitational settling.

In Section F (Fig. 10) the portion of the sill which appears to be phenocryst enriched is some 60% of the total sill thickness and the zone of maximum accumulation (as indicated by the lowest Zr and Ba values) is near the centre of the sill. The model shown in Table 4 and discussed in the previous section indicates that the residual liquids in this sill are not produced by fractionation of the phenocryst phases alone. The observations and model are consistent with flow age differentiation producing a cumulus enriched central zone and with some residual liquid being pressed out of this central zone after augite crystallisation was well advanced. The increased MgO concentration in the centre of Section E (Fig. 7) is also consistent with a mechanism of flow age differentiation. Flow age differentiation has been proposed as a fractionation mechanism in a number of other Karoo sills by Le Roex and Reid (1978) and Richardson (1979).

Conclusions

The extensive dolerite sill complex in the Huab River Valley is compositionally distinct from both the basal-

tic lavas of the overlying Etendeka Formation and from the other dolerite varieties associated with the Etendeka Formation. This, together with the locus of intrusion being close to the top of the Karoo sediments which immediately underlie the Etendeka Formation, strongly suggests that the Huab dolerites postdate the lavas (or at least the portion of the lava pile which is still preserved). This is in accord with the observations of Milner (1988) who noted that the Etendeka Formation lavas south of the Huab River were stratigraphically uplifted approximately 150 m relative to the equivalent lavas on the north side of the Huab River Valley.

Milner could not find any evidence for a fault parallel to the Huab River and suggested instead that intrusion of the Huab sills was responsible for the relative uplift.

The four dolerite types defined in this paper are distinguished from each other by different ratios of incompatible element abundances. For this reason they cannot have been derived from the same mantle source region by different degrees of partial melting and can not be related to each other by crystal fractionation processes. It is possible that some of the dolerite types have been generated by magma mixing or assimilation processes, but there is no petrographic evidence for this and the constancy of incompatible element ratios within each type suggests that such processes have not been operative to any great extent. Without isotope data for samples of each dolerite type it is not possible to model assimilation, AFC or mixing processes with adequate constraints. We conclude that on present evidence the different dolerite types in the Huab Valley are derived from mantle source regions of slightly different compositions.

Compositional variations within individual sills have been quantitatively modelled and shown to be consistent with crystal fractionation processes which appear to have operated both by gravitational separation and accumulation of early-formed phenocrysts, and by flow age differentiation.

The Huab dolerites are markedly more "primitive" in character (e.g. more magnesian and with much lower incompatible element abundances) than the basaltic lavas of the Etendeka Formation. The type-1 and type-3 dolerites have many compositional similarities to the Horingbaai dolerites which were considered by Erlank *et al.*, (1984) to have MORB characteristics and to be derived from asthenospheric mantle sources. Sr- and Nd-isotope data are required for the Huab dolerites to assess their similarities to MORB magmas in a more rigorous fashion.

Acknowledgements

This work was supported by grants from the SWA/Namibia Committee for Research Priorities, from the Foundation for Research Development, and by logistic support from the Geological Survey of Namibia. Simon Milner and Chris Harris are thanked for constructive

comments which materially improved the manuscript. The referees, Grant Cawthorn and Brian Hoal, are acknowledged for their helpful reviews.

References

- Bhattacharji, S. and Smith, C.H. 1964. Flow age differentiation. *Science*, **145**, 150-153.
- Botha, B.J.V. and Hodgson, F.D.I. 1976. Karoo dolerites in northwestern Damaraland. *Trans. geol. Soc. S. Afr.*, **79**, 186-190.
- Bougault, H. and Hekinian, R. 1974. Rift valley in the Atlantic Ocean near 36°40'N: Petrology and geochemistry of basaltic rocks. *Earth Planet. Sc. Lett.*, **24**, 249-261.
- Buddington, A.E and Lindsley, D.H. 1964. Iron-titanium oxide minerals and synthetic equivalents. *J. Petrol.*, **5**, 310-357.
- Cox, K.G. and Bell, J.D. 1972. A crystal fractionation model for the basaltic rocks of the New Georgia Group, British Solomon Islands. *Contr. Miner. Petrol.*, **37**, 1-13.
- Cox, K.G., Duncan, A.R., Bristow, J.W., Taylor, S.R. and Erlank, A.J. 1984. Petrogenesis of the basic rocks of the Lebombo. *Spec. Publ. geol. Soc. S. Afr.*, **13**, 149-169.
- Dale, I.M. and Henderson P. 1972. The partition of transition elements in phenocryst-bearing basalts and the implications about melt structure. *24th Int. geol. Congr.*, Section 10, 105-111.
- Duncan, A.R. 1987. The Karoo Igneous Province - A problem area for inferring tectonic setting from basalt geochemistry. *J. Volcanol. geotherm. Res.*, **32**, 13-34.
- Duncan, A.R, Erlank, A.J. and Betton, P.J. 1984. Appendix 1: Analytical Techniques and Database Descriptions. *Spec. Publ. geol. Soc. S. Afr.*, **13**, 389-395.
- Duncan, A R , Marsh, J.S., Milner S.C. and Erlank. A.J. 1988. Distribution and Petrogenesis of the Basic rocks of the Etendeka Formation of northwestern Namibia. *Ext. Abstr., Int. Conf. "Geochemical Evolution of the Continental Crust"*. Pocos de Caldas (Brazil), 10-19.
- Dupuy, C. and Coulon, C. 1973. Li, Rb, Sr, Ba dans les plagioclases de la suite andesitique du Logudoro et du Bosano (Sardaigne nord occidentale). *C.R. Acad. Sci. Paris*, **277**, Serie D, 1593-1596.
- Erlank, A.J., Marsh, J.S., Duncan, A.R., Miller, RMcG., Hawkesworth, C.I., Betton, P.J. and Rex, D.C. 1984. Geochemistry and Petrogenesis of the Etendeka Volcanic Rocks from SWA/Namibia. *Spec. Publ. geol. Soc. S. Afr.*, **13**, 195-245.
- Gast, P.W. 1968. Trace element fractionation and the origin of tholeiitic and alkaline magma types. *Geochim. Cosmochim. Acta*, **32**, 1057-1086.
- Gorton, M.P. 1974. *The geochemistry and geochronology of the New Hebrides*. Ph.D. thesis (unpubl.), Australian National University, 295 pp.
- Greenland, L.P. 1970. An equation for trace element distribution during magmatic crystallization. *Am. Miner.*, **55**, 455-465.
- Griffin, W.L. and Rama Murthy, V. 1969. Distribution of K, Rb, Sr and Ba in some minerals relevant to basalt genesis. *Geochim. Cosmochim. Acta*, **33**, 1389-1414.
- Hawkesworth, C.J., Marsh, J.S., Duncan, A.R., Erlank, A.J. and Norry, M.J. 1984. The role of continental lithosphere in the generation of the Karoo volcanic rocks: evidence from combined Nd- and Sr-isotope studies. *Spec. Publ. geol. Soc. S. Afr.*, **13**, 341-354.
- Hakli, T.A. and Wright, T.L. 1967. The fractionation of nickel between olivine and augite as a geothermometer. *Geochim. Cosmochim. Acta.*, **31**, 877-884.
- Hodgson, F.D.I. and Botha, B.J.V. 1975. The Karoo sediments in the vicinity of Doros, South West Africa. *Ann. geol. Surv. S. Afr.*, **10**, 49-56.
- Irving, A.J. 1978. A review of experimental studies of crystal/liquid trace element partitioning. *Geochim. Cosmochim. Acta*, **42**, 743-770.
- Kesson, S.E. 1973. The primary geochemistry of the Monaro Alkaline volcanics, southeastern Australia - evidence for upper mantle heterogeneity. *Contr. Miner. Petrol.*, **42**, 93-108.
- Leeman, W.P. and Scheidegger, K.F. 1977. Olivine/liquid distribution coefficients and a test for crystal-liquid equilibrium. *Earth Planet. Sc. Lett.*, **35**, 247-257.
- Leeman, W.P., Ma, M.-S., Murali, A.V. and Schmitt, R. A. 1978. Empirical estimation of magnetite-liquid distribution coefficients for some transition elements. *Contr. Miner. Petrol.*, **65**, 269-272.
- Le Maitre, R.W. 1981. GENMIX - A generalised petrological mixing model program. *Compo Geosci.*, **7**, 229-247.
- Le Roex, A.P. 1985. Geochemistry, mineralogy and magmatic evolution of the basaltic and trachytic lavas from Gough Island, south Atlantic. *J. Petrol.*, **26**, 149-186.
- Le Roex, A.P. and Reid, D.L. 1978. Geochemistry of Karoo dolerite sills in the Calvinia District, Western Cape Province, South Africa. *Contr. Miner. Petrol.*, **66**, 351-360.
- Miller, R.McG. 1988. 1:250 000 Geological Series 2013 Cape Cross. *Geol. Surv. Windhoek*.
- Milner, S.C. 1988. *The geology and geochemistry of the Etendeka Formation quartz latites, Namibia*. Ph.D. thesis (unpubl.), Univ. Cape Town, 263 pp.
- Paster, T.P., Schauwecker, D.S. and Haskin, L.A. 1974. The behaviour of some trace elements during solidification of the Skaergaard layered series. *Geochim. Cosmochim. Acta*, **38**, 1549-1577.
- Pearce, J.A and Norry, M.J. 1979. Petrogenetic implications of Ti, Zr, Y, and Nb variations in volcanic rocks. *Contr. Miner. Petrol.*, **69**, 33-47.
- Philpotts, J.A and Schnetzler, C.C. 1970. Phenocryst-matrix partition coefficients for K, Rb, Sr and Ba,

- with applications to anorthosite and basalt genesis. *Geochim. Cosmochim. Acta*, **34**, 307-322.
- Richardson, S.H. 1979. Chemical variation induced by flow differentiation in an extensive Karoo dolerite sheet, southern Namibia. *Geochim. Cosmochim. Acta*, **43**, 1433-1441.
- Roeder, P.L. and Emslie, R.F. 1970. Olivine-liquid equilibrium. *Contr. Miner. Petrol.*, **29**, 275-289.
- Ross, J.A. 1977. *The Tertiary Focal Peak shield volcano, south-east Queensland - A geological study of its eastern flank*. Ph.D. thesis (unpubl.), University of Queensland, 206 pp.
- Smith, H.S., Erlank, A.J. and Duncan, A.R. 1980. Geochemistry of some ultramafic komatiite lava flows from the Barberton Mountain Land, South Africa. *Precamb. Res.*, **11**, 399-415.
- South African Committee for Stratigraphy (SACS) 1980. Part I (Comp. Kent, L.E.). Lithostratigraphy of the Republic of South Africa, South West Africa/Namibia and the Republics of Bophuthatswana, Transkei and Venda. *Handb. geol. Surv. S. Afr.*, **8**, 690 pp.